Time-resolved investigation of $Cu(In, Ga)Se_2$ growth and Ga gradient formation during fast selenization of metallic precursors

R. Mainz*, A. Weber, H. Rodriguez-Alvarez, S. Levcenku,

M. Klaus, P. Pistor, R. Klenk, H.-W. Schock

Helmholt-Zentrum Berlin für Materialien und Energie,

Hahn-Meitner Plaz 1, 14109 Berlin, Germany

* Corresponding author: roland.mainz@helmholtz-berlin.de

Abstract

Ga segregation at the backside of $Cu(In, Ga)Se_2$ solar cell absorbers is a commonly observed phenomenon for a large variety of sequential fabrication processes. Here we investigate the correlation between Se incorporation, phase formation and Ga segregation during fast selenization of Cu-In-Ga precursor films in elemental selenium vapour. Se incorporation and phase formation are analysed by real-time synchrotron-based X-ray diffraction and fluorescence analysis. Correlations between phase formation and depth distributions are gained by interrupting the process at several points and by subsequent *ex situ* cross-sectional electron microscopy and Raman spectroscopy. The presented results reveal that the main share of Se incorporation takes place within a few seconds during formation of In-Se in the top part of the film, accompanied by outdiffusion of In out of a ternary Cu-In-Ga phase. Surprisingly, $CuInSe_2$ starts to form at the surface on top of the In-Se layer, leading to an intermediate double graded Cu depth distribution. The remaining Ga-rich metal phase at the back is finally selenized by indiffusion of Se. On the basis of a proposed growth model, we discuss possible strategies and limitations for the avoidance of Ga segregation during fast selenization of metallic precursors. Solar cells made from samples selenized with a total annealing time of 6.5 minutes reached conversion efficiencies of up to 14.2 % (total area, without anti-reflective coating). The evolution of the $Cu(In, Ga)Se_2$ diffraction signals reveal that the minimum process time for high quality $Cu(In, Ga)Se_2$ absorbers is limited by cation ordering rather than Se incorporation.

1 Introduction

Photovoltaic $Cu(In, Ga)Se_2$ (CIGSe) absorber layers for thin film solar cells with high energy conversion efficiency can be fabricated by reactive annealing of metallic precursor layers in selenium-containing atmosphere [1, 2]. The main challenges for a cost-efficient production of high quality CIGSe solar cells by this type of process are (i) the avoidance of highly toxic H_2Se as reaction gas, (ii) the formation of the absorber layer within short processing time, and (iii) the control of the Ga gradient during film growth. These challenges are the focus of the investigations presented in this work.

To avoid toxic H_2Se as reaction gas, Se containing precursor stacks have been used by several research groups and fabrication lines [3, 4, 5, 6]. However, a disadvantage of the use of a Se layer containing precursor is the necessity of an additional vacuum deposition step. This additional step, as well as the use of H_2Se, can be avoided by annealing Cu-In-Ga precursors in elemental Se vapour [7, 8, 9]. In this paper we show that selenization in Se vapour in connection with a fast heating ramp leads to CIGSe formation within 40 seconds. CIGSe absorbers leading to energy conversion efficiencies above 14 % were obtained within 6.5 minutes of total annealing time, making this process attractive for a cost efficient solar cell production.

In sequential chalcogenization processes, Ga segregation at the back of the film is commonly found during both selenization [10, 8, 5, 11] and sulfurization [12, 13], leading to a front band gap below the optimum and hence to a reduced open circuit voltage. In the case of CIGSe, subsequent increase of the band gap at the front can be achieved by additional sulfurization treatments [5, 14, 15], by annealing at high temperatures to allow for In-Ga interdiffusion within the selenized film [16, 10], or by a combination of both [17]. Since these additional process steps prolong the fabrication process and possibly lead to distortions of the CIGSe lattice due to a change of the lattice constant with a change of the local In/Ga or S/Se concentration, it is desirable to understand - and possibly avoid - the Ga segregation already during selenization.

Phase formation during selenization of metallic precursors [18, 19, 20, 21] as well as Ga depth distributions after selenization [16, 10, 22, 23] were investigated intensely in the past. However, the evolution of the Ga distribution during selenization of metallic precursors and its direct correlation to phase formation and Se incorporation is not yet clarified and the reasons for Ga segregation are still not fully understood.

In this work, we study the evolution of elemental depth distributions, phase formation, cation ordering, and Se incorporation during fast selenization of Cu-In-Ga precursors in elemental Se vapour by a combination of *in situ* and *ex situ* analysis methods. Synchrotron-based energy-dispersive X-ray diffraction and fluorescence analysis (EDXRD/XRF) is utilized to investigate phase formation and Se incorporation in real time. To study reaction details not accessible by *in situ* EDXRD/XRF, we interrupted identical selenization processes at several points during CIGSe growth. Raman spectroscopy on these samples reveals additional details on the phase formation and cross-

sectional electron microscopy is applied to analyse elemental depth distributions.

2 Results

2.1 Real-time phase analysis

For the real-time analysis of phase formation and Se incorporation, selenization of sputtered metallic Cu-In-Ga precursors in elemental Se vapour were performed in a closed, evacuated reaction box inside a vacuum chamber, which was tailor made for *in situ* EDXRD/XRF analysis (see Experimental Section). The Cu-In-Ga precursors with a Cu-poor composition were fabricated by sequentially sputtering In and Cu-Ga onto Mo-coated soda-lime glass. The samples were heated up to approximately 600 °C within 90 seconds, followed by an annealing step of about 5 minutes (see Experimental Section for further details).

EDXRD/XRF data recorded during selenization are presented in Fig. 1. The upper part (Fig. 1a) shows the temperature measured during the process with a thermocouple placed above the sample. Figure 1b shows colour-coded diffraction and fluorescence signal intensities as function of photon energy and process time. At room temperature, diffraction signals of Mo, In and of a further metallic phase referred to as $Cu_x(In, Ga)_y$ are found, resulting from the precursor fabrication by sequential sputtering. The positions of the reflexes attributed to $Cu_x(In, Ga)_y$ coincide with those reported for the closely related hexagonal $Cu_{16}(In, Ga)_9$ and cubic $Cu_9(In, Ga)_4$ phase [13, 24, 25]. Since the cubic phase features additional reflexes [13] which are not observed here, we assume that $Cu_x(In, Ga)_y$ corresponds to hexagonal $Cu_{16}(In, Ga)_9$. Upon heating, the diffraction signals of In disappear in accordance to the melting point of In at about 150°C. At this point, In is assumed to be incorporated into the $Cu_x(In, Ga)_y$ phase as the intensity of the $Cu_x(In, Ga)_y$ reflex at 39 keV is slightly increasing. However, the solubility of In in $Cu_x(In, Ga)_y$ at high temperatures is not well known, and thus we cannot exclude that some In is present in the liquid state.

Presence of indium selenides, In_4Se_3 and InSe, can be observed for a few seconds together with the metallic $Cu_x(In, Ga)_y$ phase. The disappearance of the indium selenides and the metallic $Cu_x(In, Ga)_y$ phase correlates with a fast increase of several reflexes that can be attributed to chalcopyrite CIGSe. During further annealing of the film, slow formation of $MoSe_2$ can be observed, starting approximately 1 minute after the formation of CIGSe.

Around the expected position of CIGSe 112, two distinct reflexes can be discerned in Fig. 1b: a strong reflex near the position of $CuInSe_2$ (CISe) 112 and a weak reflex at the position of $CuGaSe_2$ (CGSe) 112. This can be seen in more detail in Fig. 1c, which shows single spectra extracted from the real-time data at points in time and in the energy range marked by the short vertical lines (A-D) in Fig. 1b. The asymmetric broadening of the CIGSe 112 signal [26, 27, 28] indicates an In-Ga segregation immediately when the chalcopyrite phase started to form. However, it is noted that the attribution of the

weak signal to CGSe 112 is not unique since it coincides with the position of CISe 103. The formation of CGSe is investigated in more detail by cross-sectional SEM in Section 2.4. The decrease of the peak at the CGSe 112 position from A-C can be explained by In-Ga interdiffusion [28], whereas the increase of a new peak at slightly higher energies (D) compared to that of CGSe 112 and CISe 103 can be explained by the rise of CIGSe 103 caused by increasing cation ordering (see next section).
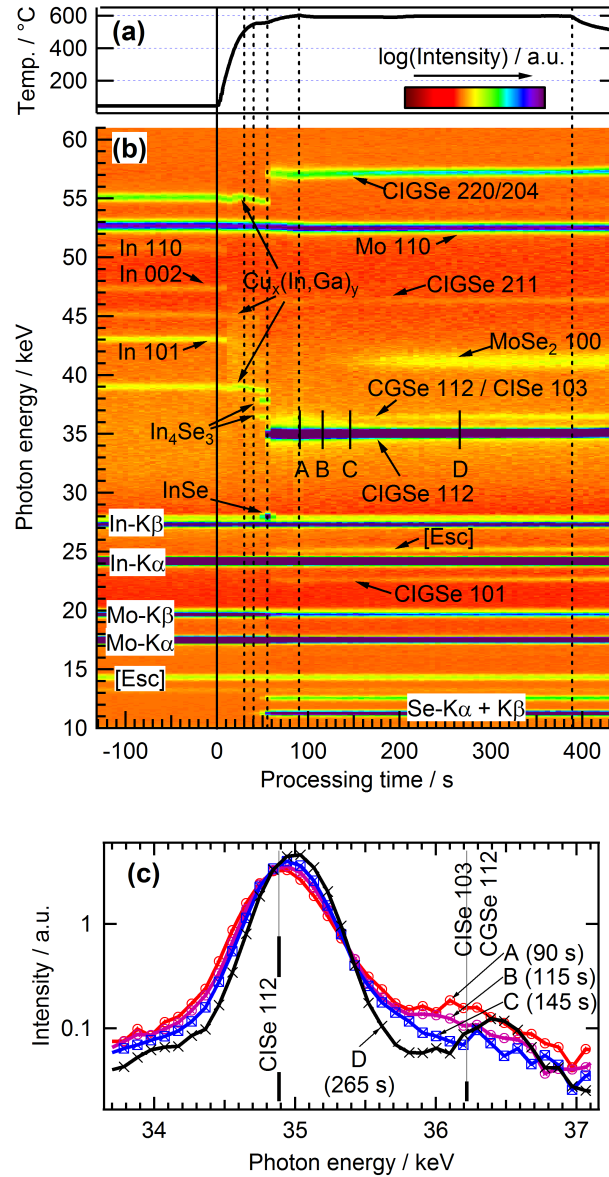

Figure 1: Time-resolved EDXRD/XRF analysis during annealing of a Cu-In-Ga precursor film in Se vapour. a) Temperatures measured by a thermocouple placed 5 mm above the sample. b) Color-coded diffraction signals as function of photon energy and process time (CIGSe: $Cu(In, Ga)Se_2$; CGSe: $CuGaSe_2$; [Esc]: escape peak caused by the Ge-K edge of the Ge detector). All spectra are normalized to the In-Kα fluorescence intensity. (c) Subrange of single EDXRD spectra retrieved from (b) at various points in time during the annealing plateau. The points in time and the energy ranges of the spectra (A-D) are marked as vertical lines in (b). The vertical lines in this figure mark expected positions for $CuInSe_2$ (CISe) 112, $CuInSe_2$ 103, and $CuGaSe_2$ (CGSe) 112

4

2.2 Se incorporation and cation ordering

Evolutions of integral signal intensities extracted from the real-time EDXRD/XRF data by peak fitting are shown in Fig. 2a and b. Fig. 2a reveals that the main share of Se incorporation - detected by the increase of the Se-Kα signal - correlates with In-Se formation and occurs within 20 sec. Subsequent formation of CIGSe during consumption of InSe and $Cu_x(In, Ga)_y$ occurs within 10 sec. The total time needed for the selenization of the film is approximately 40 seconds.

We note that in an additional heating process without Se, the $Cu_x(In, Ga)_y$ disappears at higher temperatures at the end of the heating stage (grey, dashed line in Fig. 2a). This observation can be explained by formation of a liquid Cu-In-Ga phase and thus provides important information for the design of selenization processes with controlled Se supply, because melting of metal phases possibly leads to dewetting. To avoid this it is likely that Se vapour must be supplied before melting of the metal phase.

The fast rise of the main CIGSe reflex 112, 220/204, and 312/116 to their maximum values (Fig. 2a,b) indicates fast formation of a CIGSe phase with a zinc-blende type Se sublattice, as found in the chalcopyrite structure. However, it is important to note that these main reflexes are not sufficient for a unique identification of chalcopyrite-type CIGSe since they could also origin from a cubic zinc-blende type structure with random
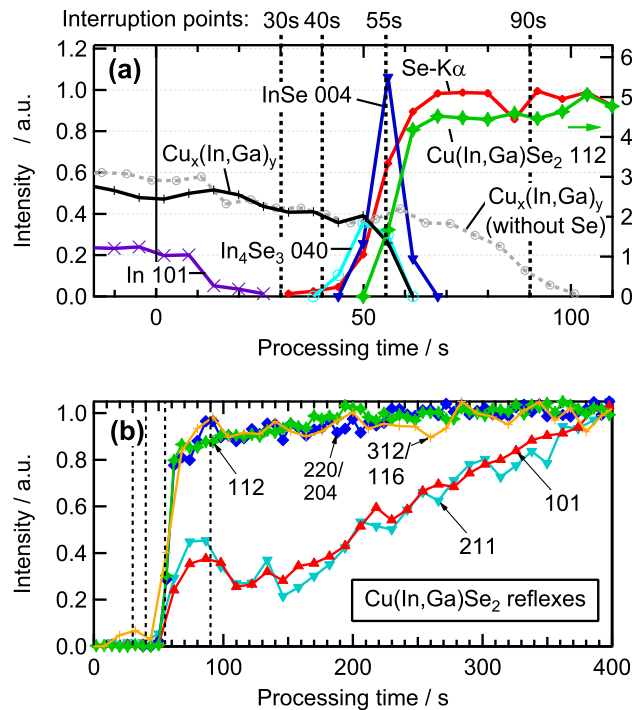

Figure 2: Evolution of integral intensities extracted from the EDXRD/XRF data in Fig. 1. (a) Evolution of intensities of the Se fluorescence signal (Se-Kα) and selected diffraction signals during selenization. The grey, dashed line in (a) presents the intensity of $Cu_x(In, Ga)_y$ recorded during annealing without selenium atmosphere. All signals were divided by the intensity of In-Kα. (b) Evolution of normalized intensities of $Cu(In, Ga)Se_2$ diffraction signals throughout the complete process.

distribution of Cu and In or Ga on the cation sites. In contrast, the occurrence of the weak 101 and 211 reflexes (Fig. 2b) reveals formation of tetragonal CIGSe with cation ordering in the chalcopyrite structure [29]. A transition from random to ordered cation site occupation leaves the average In and Cu occupancy of the (112), (220)/(204) and (312)/(116) planes and hence their scattering intensities unaffected. In contrast, cation ordering strongly changes the average occupancy in the (101), (103) and (211) planes. In a completely random In and Cu distribution over the cation sites, the 101, 103 and 211 diffraction lines were cancelled out. Consequently, the rise of the intensities of these weak reflexes relative to the intensities of the main reflexes can be explained by increasing cation ordering. In contrast to kesterite Cu_2ZnSnS_4 [30], the equilibrium state of chalcopyrite CIGSe at 600 °C has completely ordered cation site occupation [31]. The evolution of normalized intensities of the weak 101, and 211 reflexes as well as those of the main reflexes are depicted in Fig. 2b. While the main reflexes rise within around 20 seconds, the weak reflexes - after an initially fast increase coinciding with the main reflexes - show a subsequent slow increase throughout the remaining annealing time of ~5 min. at 600 °C. Thus, the time-resolved increase of the weak reflexes shown here provide insight into the dynamics of the cation ordering within the Se sublattice. The fact that their intensities are still increasing near the end of the annealing time suggests that complete cation ordering was not yet reached at the end of the process. Possible consequences of cation disorder on the solar cell performance will be discussed at the end of Sec. 3.

2.3 *Ex situ* Raman phase analysis

Whereas the main increase of the Se fluorescence signal (Se-Kα) correlates with the formation of the indium selenides (In_4Se_3 and InSe), a weak increase of Se-Kα even several seconds before indium selenides can be detected (Fig. 2a). This indicates the formation of an additional selenide phase that is not detected by real-time diffraction. To gain additional insight into the presence of phases, identical processes were interrupted after 30, 40, 55, and 90 s during heating and the intermediate states were analysed by *ex situ* angle-dispersive XRD and Raman. The points of process interruptions are marked as vertical lines in Figs. 1a, 2a and 2b. Standard *ex situ* XRD measurements (not shown) of the samples resulting from the interrupted processes match the phases observed by real-time EDXRD. In contrast, the Raman shows a strong peak at 261 cm^{-1} for the sample interrupted at 40 s (Fig. 3), which coincides with a vibrational mode of $Cu_{2-x}Se$ [32]. Thus, we interpret the weak rise of Se-Kα between 30 and 40 s processing time (Fig. 2a) to be partially caused by the formation of $Cu_{2-x}Se$. After 55 s the $Cu_{2-x}Se$ has disappeared again. Note that a detection of the indium selenides by Raman spectroscopy would require measurements in the low wavelength region (<150 cm^{-1}), where the strongest Raman active modes were reported [33, 34].

The Raman measurements reveal additional phase details that were not accessible by diffraction. Besides a peak at 174 cm^{-1}, which can be attributed to CuInSe$_2$ [32], a broad
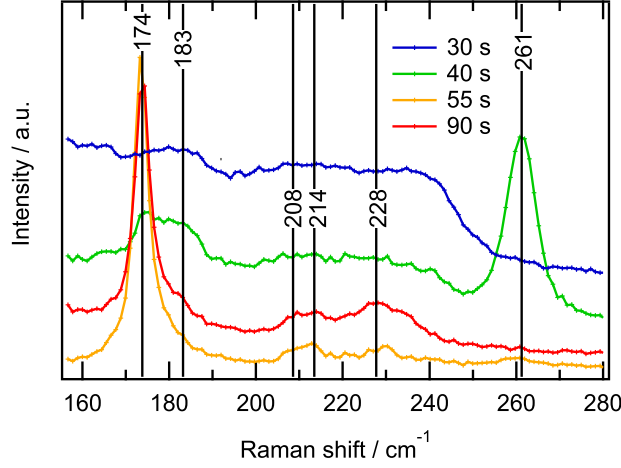
Figure 3: Raman measurements performed on the samples resulting from selenization processes that were interrupted after 30 s, 40 s, 55 s, and 90 s. The peak at $261\,\mathrm{cm}^{-1}$ indicates the presence of $Cu_{2-x}Se$.

peak at 183 cm^{-1} can be identified after 40 s. It is known that Cu-deficient Cu-In-Ga-Se compounds crystallize in chalcopyrite based structures with point defects like In_{Cu} or Ga_{Cu} as ordered vacancy compounds (OVC) [35]. These compounds may comprise different compositions, e.g. $Cu(In, Ga)_5Se_8$ or $Cu(In, Ga)_3Se_5$. For $Cu(In, Ga)_5Se_8$ a main peak at 150 cm^{-1} and a weaker one at about 185 cm^{-1} have been reported by Caballero et al. and Xu et al. [35, 36]. Consequently, the 183 cm^{-1} peak, which is already visible at 30 seconds, may be attributed to an OVC phase. With further processing (at 55 s and 90 s) the signal at 183 cm^{-1} significantly weakens. The newly appearing peaks at about 208 cm^{-1}, 214 cm^{-1} and 228 cm^{-1} can be attributed to chalcopyrite CIGSe [37].

2.4 Evolution of depth distributions

The asymmetric peak shape of the CIGSe 112 reflex observed in the *in situ* EDXRD signals indicated a segregation of Ga right at the beginning of the CIGSe phase formation (Fig. 1). Additionally, the formation of In-Se prior to CIGSe suggests that In-Ga separation starts even before the formation of CIGSe (Fig. 2a). To be able to understand these observations in detail, elemental depth distributions were analysed by SEM and EDS. The left hand side of Fig. 4 shows SEM images of cleaved cross-sections of the samples resulting from the process interruptions. The graphs in the centre show EDS line scans gained by integration over the lateral range marked by the rectangle in the SEM images. (We note that the analysed films featured lateral inhomogeneities of the Ga/In distributions within the metallic bottom layer. This might be caused by phase separation in the metallic phase due to limited Cu-In-Ga miscibility at low temperatures.)

The first EDS line scan reveals presence of selenium in the top part of the film already after 30 s (Fig. 4a, centre). However, the main part of the film shows a metallic layer with nearly homogeneous depth distributions of Cu, In, and Ga. This confirms that most
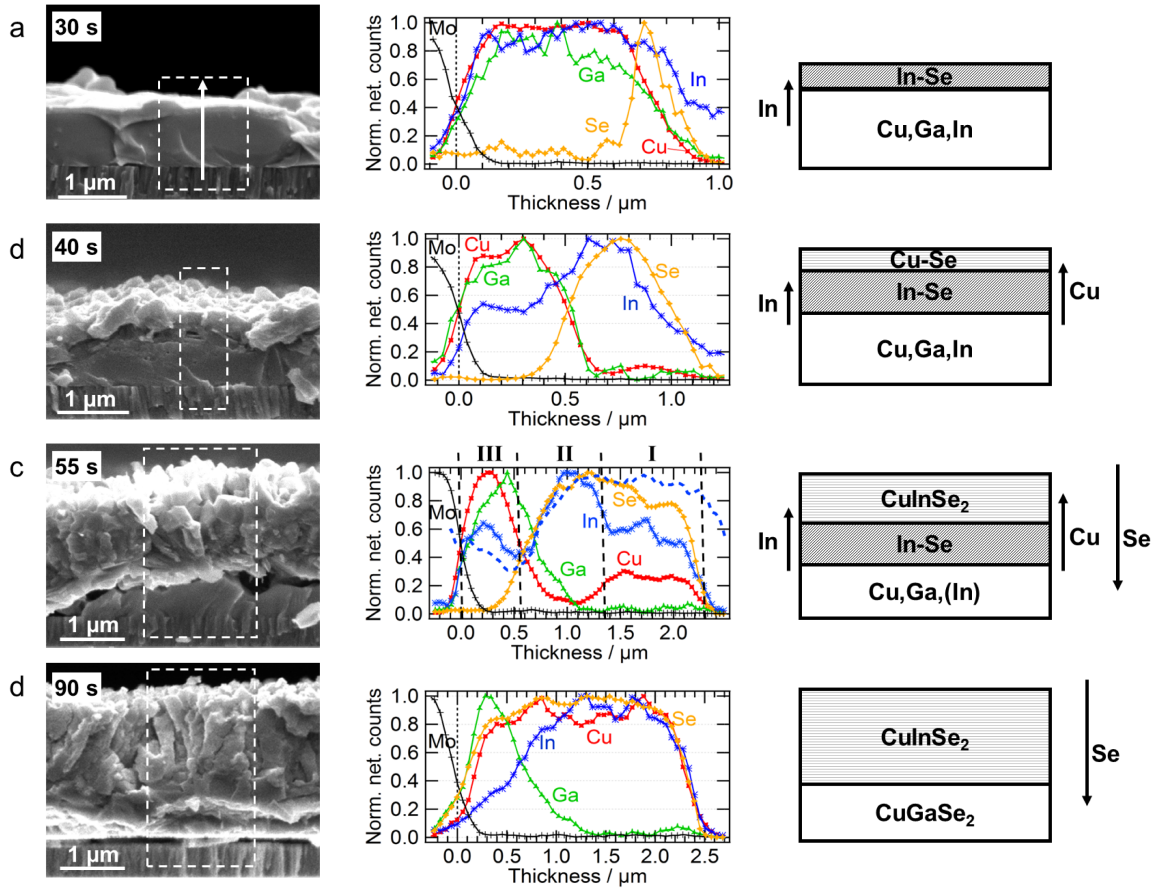
7

Figure 4: SEM images (left) and SEM-EDS linescans (centre) of cleaved cross-sections of the samples interrupted after (a) 30 s, (b) 40 s, (c) 55 s, and (d) 90 s of the selenization of metallic Cu-In-Ga precursor films. The EDS intensities were gained by integrating over a lateral range marked by the dashed rectangles in the SEM images. The dashed blue line in (c) presents the ratio In/(Ga+In) calculated from the normalized net counts and the arrow in the first SEM image indicates the direction of the corresponding line scan. The drawings on the right show simplified schematic presentations of the depth distributions and phases observed by EDS and diffraction.

of the In from the sputtered In layer was incorporated into the $Cu_x(In, Ga)_y$ phase at the beginning of the heating process.

After 40 s, a 400 nm thick top layer consisting of mainly In and Se as well as some Cu can be discerned (Fig. 4b). Simultaneously, the thickness of the metallic bottom layer decreased (note the different scalings of the x-axes of the EDS line scans). In contrast to In, Ga completely remained in the metallic layer at the back of the film and the Ga/In ratio within this metallic layer increased. The EDS signal of Cu shows a small maximum at the surface region which is consistent with the observation of $Cu_{2-x}Se$ by Raman.

After 55 s, the film can be subdivided in three distinct layers (Fig. 4c, centre): (I) A top layer consisting of Cu, In and Se; (II) a middle layer mainly consisting of In and Se and with a low Cu concentration; and (III) a metallic bottom layer consisting of Cu, In, and Ga. The real-time EDXRD, as well as the Raman data measured on the same sample, suggest that the top layer consists of chalcopyrite $CuInSe_2$ (Fig. 2a and Fig. 3). Still no

8

Ga can be detected in the top part of the selenized layer, while some Ga diffused from the bottom layer (III) into the In-Se layer (II) forming a steep gradient. In comparison to the state after 30 s, the Ga/In ratio in the metallic bottom layer increased from about 0.3 to 0.6, according to the absolute EDS intensities. It is noteworthy that the In/(Ga+In) distribution within the metallic layer is not homogeneous any more, but features a gradient with a minimum In concentration at the metal/selenide interface (dashed blue line).

Finally, the film that was heated for 90 seconds shows complete selenization of the film (Fig. 4d), which is in accordance with the real-time signal intensities in Fig. 2a. The EDS data show strong Ga enrichment at the back of the selenized film. By comparing the EDS data from Fig. 4a-d (30 s to 90 s), it can be seen that Ga stays in the metallic phase at the bottom until Se reaches this part of the film, finally leading to complete selenization.

2.5   Solar cell characterization

Absorbers grown with the process type depicted in Fig. 1 were finished to solar cells (no anti-reflective coating was used; see Experimental Section for details). Current-voltage characteristics of the best solar cell resulting from this process are shown in Fig. 5a. The cell exhibits high fill factor and current, while the open circuit voltage is rather low for CIGSe. Fig. 5b depicts external quantum efficiency of the same solar cell. On the high wavelength side, the steepest slope is at approximately 1.0 eV. The band gap is therefore close to that of CuInSe$_2$ [38]. This is in accordance with a Ga-poor top layer of the CIGSe absorber as seen in Fig. 4d. Even though the annealing plateau at 600 °C leads to some In-Ga interdiffusion, the surface of the film remains very Ga-poor [39]. It is noteworthy that a reduction of the annealing plateau from 5 min. to 2.5 min. leads to a reduction of V_{oc} by about 80 mV. Possible reasons for this difference are discussed in Sec. 3.

We note that 2.5 % of sulphur was found in the bottom part of the absorber of the solar cell, most likely resulting from residuals in the annealing chamber.

3   Discussion

The evolution of phases and elemental depth distributions during selenization of the metallic precursor film is governed by an interplay of solid-state reactions and diffusion. Once a first selenide layer has formed at the surface of the metallic layer, further reaction necessarily involves either diffusion of metals through this layer towards the surface of the sample, or diffusion of selenium towards the back - or a combination of both. Within the complete temperature range of the process, Cu(In, Ga)Se$_2$ is the most stable phase of the quaternary system in equilibrium [40]. Therefore, all intermediately formed phases are a result of kinetic limitations.

The reaction path identified by real-time EDXRD, Raman spectroscopy and cross-sectional EDS is schematically summarized in Fig. 4 (right). During selenization, the
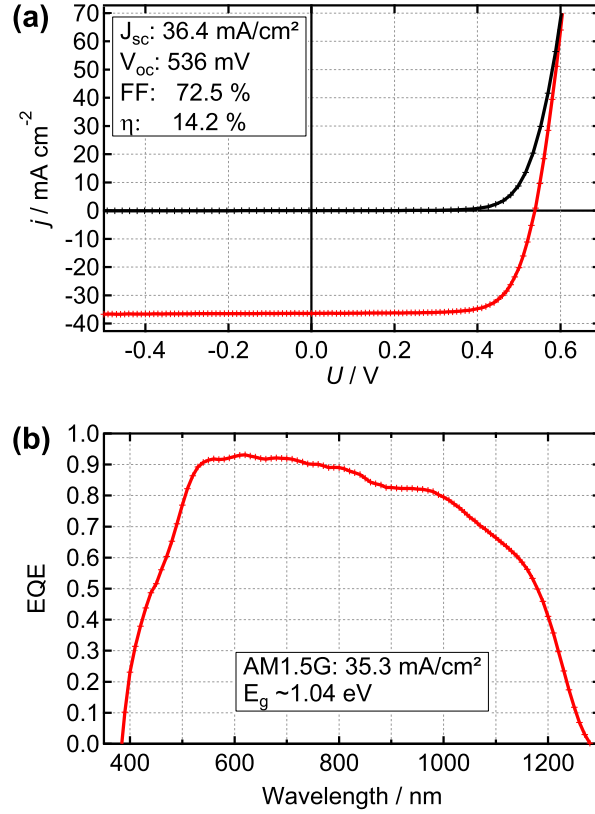
Figure 5: (a) Dark (black line) and light (red line) current-voltage measurements of the best solar cell from a absorber grown by selenization of a Cu-In-Ga precursor in Se vapour. A least square fit of the 1-diode model to the data measured in the dark (black line) gave a diode factor $A = 1.67$, saturation current $j_0 = 7 \cdot 10^{-5}\,\mathrm{mA\,cm^{-2}}$, and serial and parallel resistance $R_s = 0.13\,\Omega\,\mathrm{cm^2}$ and $R_p = 7.4\,\mathrm{k\Omega\,cm^2}$. (b) External quantum efficiency of the same solar cell.

first selenide phases that are detectable are indium selenides and copper selenide, which were also found by others during selenization in H_2Se [25, 17] or metal/Se stacks [18]. In the very beginning of the process, the first thin layer of In-Se might be formed from excess In that was not incorporated into the ternary $Cu_x(In, Ga)_y$ phase after the melting of the solid In layer of the precursor film. Our analysis of the depth distributions showed that during further In-Se formation In is consumed from an initially homogeneous metallic $Cu_x(In, Ga)_y$ phase (Fig. 4a,b). The formation of an In/(Ga+In) gradient within the metal layer (dashed line in Fig. 4c, centre, section III) is in accordance with the picture of outdiffusion of In during In-Se formation, leading to a decrease of the In concentration at interface between the metal layer and the selenide layer. Additionally it reveals that the reaction of In with Se is - at least partially - limited by the diffusion of In within the metal layer, since otherwise the In gradient in the metal layer would be flat. In principle, with an increase of the Ga/In ratio in the $Cu_x(In, Ga)_y$ phase a decreasing lattice parameter [24, 13, 25] and hence a shift of the diffraction signals to higher energies [13] would be expected, which is not observed here. On the one hand, some lattice contraction can be partially overcompensated by thermal expansion during the heating stage. On the

other hand, the overall Cu-poor composition can - in contrast to Ref. [13] - lead to a decreasing Cu concentration, eventually causing segregation of a liquid Cu-Ga phase at high temperatures [41] which would not be seen in the real-time diffraction measurements.

Remarkably, in the further course of the reaction, the Cu concentration forms a double graded depth profile (Fig. 4c, centre) - with a high Cu concentration in the metallic bottom part (III), a low Cu concentration in the middle part in which mainly In and Se are present (II), and an increased Cu concentration in the top part of the film where In, Se, and Cu are present (I). This reveals that Cu diffuses from the metal layer through the In-Se layer to the front to form $CuInSe_2$. The question at hand is: Why does Cu not react with In and Se to $CuInSe_2$ right at the metal/In-Se interface where sufficient Cu is available? To understand this behaviour, it is important to note that the Se/In ratio of $CuInSe_2$ is higher than that of In_4Se_3 or InSe and therefore the formation of $CuInSe_2$ from these In-Se phases needs - besides Cu - also additional Se:

$$InSe + Cu + Se \rightarrow CuInSe_2$$
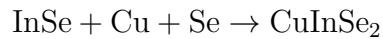
Consequently, for $CuInSe_2$ formation at the metal/In-Se interface, either Se from the surface would need to diffuse through the In-Se layer to the metal/In-Se interface, or In would need to diffuse away from the interface to increase the Se/In ratio and thus allow $CuInSe_2$ formation. In contrast, for $CuInSe_2$ formation at the surface, sufficient Se supply is available from the gas phase. In this case, only Cu needs to diffuse through the In-Se layer to form $CuInSe_2$ at the surface. Therefore, from the observation that $CuInSe_2$ forms on top of the In-Se layer, we can conclude that

- Cu is soluble to a certain extent in In-Se - thus enabling Cu diffusion through In-Se,

- Cu has a higher diffusivity in In-Se than Se and In.

Basically no Ga contributes to this early formation of the chalcopyrite phase. The main part of the Ga accumulation, however, takes place already during In-Se formation, leading to an increase of the Ga/In ratio in the remaining metal layer at the back of the film. The prevalence of In-Se formation over Ga containing phases can, in principle, be due to both, a lower activation energy for In-Se formation compared with other phases - as proposed by Hanket et al. [25] - or higher diffusivity of In compared with that of Ga [42]. From the presented data, it is not clear if the initially preferred reaction of In with Se over Ga with Se is due to limited Ga diffusivity or due to a higher reactivity of In compared with Ga. However, the fact that Ga stays at the back during transition from the remaining metal Cu-Ga phase to $CuGaSe_2$ (Fig. 4c,d) shows that for this reaction Se diffuses to the back of the film instead of Ga and Cu diffusing to the surface. Since Cu is known to be very mobile in CIGSe [43, 44] and thus it can be assumed that the reaction is not limited by Cu diffusion, this observation reveals that

- Ga has a lower mobility in CIGSe than Se.

On the basis of these considerations, we can distinguish two distinct growth regimes: In the first regime the metal atoms In and Cu diffuse to the front and react with Se to form binary and ternary selenides (Fig. 4a-c). In the second growth regime, Se diffuses through the selenide layer and reacts with the metals Cu and Ga in the bottom part of the film (Fig. 4c-d). These two growth regimes are depicted schematically in Fig. 6. Which growth regime applies depends on the differences in the diffusion currents of selenium and the metals as well as on activation energies for the reactions. If growth regime 1 applies for In and growth regime 2 applies for Ga, this will unavoidably lead to a separation of In and Ga during selenization. Thus, it seems that Ga segregation during selenization can only be avoided or reduced if either the reaction of Ga is shifted towards growth regime 1, or the reaction of In is shifted towards growth regime 2.

Figure 6: Schematic models for film growth for the case of 1) prevailing metal diffusion and of 2) prevailing selenium diffusion. The growth front is marked red.

In the first case - i.e. growth regime 1 holds for both In and Ga and the CIGSe growth front is at the surface - Ga segregation will only be avoided if the diffusion current of In and Ga to the surface, as well as their reaction rate with Se, are equal. According to our results, an equal diffusion coefficient for In and Ga in CIGSe cannot be expected. Then, the only way to obtain an equal reaction rate of In and Ga with Se at the surface is to slow down the reaction at the surface such that the cations have sufficient time to diffuse to the front, guaranteeing that the reaction rate is not limited by diffusion. A way to achieve this could be to lower the Se partial pressure such that the reaction is limited by the availability of Se at the surface rather than by In and Ga diffusion.

For the second case - i.e. growth regime 2 applies for both In and Ga - the metals would not diffuse at all. Then, the composition of the metals at the growth front between CIGSe and metal layer could stay constant and In-Ga segregation would be avoided, given that CIGSe growth is not limited by the reactivity of In and Ga but rather by the indiffusion of Se. If the temperature dependence of the diffusion of Se is different from those of the metals, an alteration of the process temperature may help to shift the reaction towards growth regime 2. Recent results presented by Wang et al. suggest that a pre-annealing at very low temperatures (130-200 °C) might move into this direction, unfortunately also connected with very long total processing times of about 2 hours [45].

If these two strategies do not succeed to prevent or reduce Ga segregation during CIGSe growth from metallic precursors, deposition of Se already in the precursor layer seems to be the remaining strategy to avoid Ga segregation during growth [46, 47, 45, 48]. The drawback of this approach, however, is that up to now it required long annealing times

of around one hour [49, 50, 51] to achieve efficiencies of up to 13.2 % [51]. In contrast, in the fast selenization process of pure metallic precursors presented in this work, efficiencies of up to 14.2 % were already achieved within 6.5 minutes total processing time, despite Ga accumulation at the back of the film. A possible reason for the need of long annealing when starting with Se-containing precursors could be that annihilation of Se defects - possibly formed during precursor deposition - takes much longer time than annihilation of cation defects. In process investigated here, annihilation of cation disorder defects was found to take place within only a few minutes.

If Ga segregation cannot be avoided during selenization of purely metallic precursors, a flattening of the Ga gradient can be achieved by In-Ga diffusion subsequent to CIGSe formation [16, 10], which partially also takes place during the annealing stage of the process investigated here. An inherent problem of this strategy could be that lattice defects form at the initially steep Ga gradient [52] and additional stress induced lattice defects may form during diffusion of Ga out of the initially Ga-rich layer and into the initially In-rich layer due to the dependence of the lattice parameters on the In/Ga ratio. These aspects form a strong motivation for avoidance of strong Ga segregation already during CIGSe growth.

It is worth to emphasize that in the fast selenization process investigated here, the transformation from CIGSe with partially disordered cation occupation to the ordered chalcopyrite structure is the most time consuming reaction step and therefore governs the minimum time needed to produce high-quality chalcopyrite CIGSe absorbers films. Cation disorder may strongly affect the electronic properties of CIGSe such as a decreased band gap energy [53]. Thus, partial cation disorder can be expected to lead to detrimental band gap fluctuations and reduced open circuit voltage. The observed increase in open circuit voltage with increasing length of the temperature plateau at 600 °C from 2.5 to 5 min. could therefore be caused by an increasing cation ordering. The voltage increase could, however, also be caused by an increased surface band gap due to Ga diffusing to the surface. To isolate the effect of cation ordering from In-Ga interdiffusion, further experiments with CIGSe absorbers possessing flat Ga distribution or no Ga are necessary.

4   Conclusion

We have demonstrated the potential of a fast selenization process of metal precursors in elemental Se atmosphere for the fabrication of well performing photovoltaic absorbers within 6.5 minutes, avoiding the use of toxic H_2Se and Se deposition onto the precursor. Solar cells made from absorbers synthesized by this kind of process showed efficiencies of up to 14.2 % despite Ga deficiency in the front part of the film. Real-time *in situ* measurements revealed that the main selenization reaction occurs within a few tens of seconds, while subsequent ordering of the cations for the formation of the chalcopyrite structure takes up to 5 minutes. We found that during selenization, Ga accumulation

starts to form by a Ga enrichment of the metallic phase while CuInSe$_2$ is formed on top of an indium selenide layer. Based on our reaction model we propose that during selenization of metallic precursors, Ga accumulation could only be avoided or reduced either if the reaction is slowed down such that reaction rate at the surface is not limited by diffusion any more, or if the diffusion current of Se into the film relative to the outdiffusion of the metals can be increased.

5   Experimental Section

Precursors: The Cu-In-Ga films used for the selenization processes were deposited on Mo-coated soda-lime glass by successive DC sputtering of a 464 nm thick In layer and a 252 nm thick Cu-Ga layer from a Cu$_{85}$Ga$_{15}$ alloy target. The resulting composition of the precursor film was analysed by X-ray fluorescence analysis (XRF) and gave a Cu/(In+Ga) ratio of about 0.75.

Selenization: Selenization and anealing experiments were performed in a reaction box inside a vacuum chamber, which was tailor made for *in situ* EDXRD/XRF measurements at the polychromatic EDDI beamline of the BESSY II synchrotron source [54]. The reaction box consists of a graphite ring and a quartz glass bottom and lid plate. Cu-In-Ga precursor samples were placed inside the reaction box. Se pellets were placed next to the samples inside the reaction box. The atomic ratio of the Se pellets to the precursor metals was approximately 2.5. Prior to heating, the box was evacuated to a pressure below $5 \cdot 10^{-4}$ mbar. Subsequently, the box was closed by a valve. The samples were heated up to approximately 600 °C within 90 seconds, followed by an annealing step of about 5 minutes. Heating was realized by 8 halogen lamps - 4 above and 4 below the reaction box - with a total maximum power of 4000 W. The selenium was heated together with the precursor samples. After the end of the heating step, the valve of the reaction box was opened for 5 seconds to reduce Se pressure during the annealing step.

Real-time EDXRD/XRF: During the selenization process, the samples were irradiated by collimated polychromatic synchrotron radiation of the EDDI beamline at BESSY II. EDXRD/XRF spectra were recorded by an energy-dispersive Ge detector under a diffraction angle $2\theta = 6.10°$ and with a time resolution of 5 s. The relationship between the photon energy of a diffraction reflex E_{hkl} and the corresponding lattice plane distance d_{hkl} of a crystalline phase follows the energy-dispersive form of the Bragg equation, $E_{hkl} = hc/(2d_{hkl}\sin(\theta))$, where h is Planck's constant and c the speed of light. For further details on the experimental set-up see Ref. [55]. Integral signal intensities were determined by multi-peak fitting using Voigt profiles. Crystalline phases observed by EDXRD were identified by comparing the energy positions of the observed signals with the energies calculated from XRD reference patterns by the energy-dispersive form of the Bragg equation (see above). Reference patterns were taken from the database of the International

Centre for Diffraction Data (ICDD) with the following PDF card numbers: In: 5-0642; In_4Se_3: 051-0808; InSe: 034-1431; $CuInSe_2$: 81-1936; $CuGaSe_2$: 81-0903; $MoSe_2$: 29-0914.

***Ex situ* characterization:** Identical selenization processes were repeated several times and interrupted at various points in time to study intermediate states by Raman and by cross-sectional energy-dispersive X-ray spectroscopy in a scanning electron microscope (EDS-SEM). The process interruptions were realized by turning off the heating lamps resulting in a passive cool down of the substrates. A Leo1530 microscope was used for scanning electron microscopy (SEM) and energy dispersive X-ray spectroscopy (EDS) at an acceleration voltage of 7 kV. The Raman measurements were performed with DILOR LabRam Micro-Raman system in the back-scattering geometry at room temperature. A He-Ne laser light at 632.8 nm was focused with an objective lens 50x (NA=0.75) on the sample. A silicon mode at 520.7 cm^{-1} was used for the frequency calibration.

Solar cells: Selenized absorbers were processed to solar cells by etching in KCN, chemical bath deposition of CdS, sputtering of undoped and Al-doped ZnO and finally deposition of Ni/Al grid fingers. Anti-reflective coating was not used. Finished solar cells had a size of 0.5 cm^2 and were characterised by quantum efficiency and IV measurements under simulated AM1.5 illumination.

Acknowledgements

References

[1] Probst, V., Stetter, W., Riedl, W., Vogt, H., Wendl, M., Calwer, H., Zweigart, S., Ufert, K.-D., Freienstein, B., Cerva, H., and Karg, F. H. Rapid CIS-process for high efficiency PV-modules: development towards large area processing. *Thin Solid Films* **387**, 262–267 (2001), doi: 10.1016/S0040-6090(00)01800-9.

[2] Solar Frontier, press release (accessed 25.10.2013): http://www.solar-frontier.com/eng/news/2013/c014763.html.

[3] Palm, J., Probst, V., and Karg, F. H. Second generation CIS solar modules. *Solar Energy* **77**(6), 757–765 (2004), doi: 10.1016/j.solener.2004.05.011.

[4] Kötschau, I. M., Kampmann, A., Hahn, T., Hinze, J., Pursche, O., Gorse, S., and Richter, E. A new reactive annealing approach for large scale $Cu(In,Ga)Se_2$ mass production. In *24th European Photovoltaic Solar Energy Conference and Exhibition, Hamburg, Germany*, 3DO.6.1, (2009), doi: 10.4229/25thEUPVSEC2010-3BV.2.139.

[5] Kulkarni, S., Koishiyev, G., Moutinho, H., and Dhere, N. Preparation and characterization of $CuIn_{1-x}Ga_xSe_{2-y}S_y$ thin film solar cells by rapid thermal processing. *Thin solid films* **517**, 2121–2124 (2009), doi: 10.1016/j.tsf.2008.10.128.

[6] Hsu, C.-Y., Huang, P.-C., Chen, Y.-Y., and Wen, D.-C. Fabrication of a $Cu(InGa)Se_2$ thin film photovoltaic absorber by rapid thermal annealing of CuGa/In precursors coated with a Se layer. *International Journal of Photoenergy* **2013**, 132105 (2013), doi: 10.1155/2013/132105.

[7] Kim, W., Payzant, E. A., Li, S., Crisalle, O., and Anderson, T. In-situ observation of selenization of Cu-Ga-In metallic precursors. In *Photovoltaic Energy Conversion, Conference Record of the 2006 IEEE 4th World Conference*, volume 1, 453–456, (2006), doi: 10.1109/WCPEC.2006.279488.

[8] Caballero, R., Guillén, C., Gutiérrez, M. T., and Kaufmann, C. A. $CuIn_{1-x}Ga_xSe_2$-based thin-film solar cells by the selenization of sequentially evaporated metallic layers. *Prog. Photovolt: Res. Appl.* **14**(2), 145–153 (2006), doi: 10.1002/pip.649.

[9] Li, W., Sun, Y., Liu, W., and Zhou, L. Fabrication of $Cu(In,Ga)Se_2$ thin films solar cell by selenization process with Se vapor. *Solar Energy* **80**(2), 191–195 (2006), doi: 10.1016/j.solener.2005.07.011.

[10] Marudachalam, M., Birkmire, R. W., Hichri, H., Schultz, J. M., Swartzlander, A., and Al-Jassim, M. M. Phases, morphology, and diffusion in $CuIn_xGa_{1-x}Se_2$ thin films. *J. Appl. Phys.* **82**(6), 2896–2905 (1997), doi: 10.1063/1.366122.

[11] Ru Hsu, H., Chun Hsu, S., and Liu, Y.-s. Improvement of Voc and Jsc in $CuInGaSe_2$ solar cells using a novel sandwiched CuGa/CuInGa/In precursor structure. *Appl. Phys. Lett.* **100**(23), 233903 (2012), doi: 10.1063/1.4705297.

[12] Neisser, A., Hengel, I., Klenk, R., Matthes, T. W., Álvarez García, J., Pérez-Rodríguez, A., Romano-Rodríguez, A., and Lux-Steiner, M. C. Effect of Ga incorporation in sequentially prepared $CuInS_2$ thin film absorbers. *Sol. Energy Mater. Sol. Cells* **67**(1-4), 97–104 (2001), doi: 10.1016/S0927-0248(00)00268-3.

[13] Mainz, R., Klenk, R., and Lux-Steiner, M. Sulphurisation of gallium-containing thin-film precursors analysed in-situ. *Thin Solid Films* **515**(15), 5934–5937 (2007), doi: 10.1016/j.tsf.2006.12.167.

[14] Nagoya, Y., Kushiya, K., Tachiyuki, M., and Yamase, O. Role of incorporated sulfur into the surface of Cu(InGa)Se$_2$ thin-film absorber. *Sol. Energy Mater. Sol. Cells* **67**(1-4), 247–253 (2001), doi: 10.1016/S0927-0248(00)00288-9.

[15] Probst, V., Palm, J., Visbeck, S., Niesen, T., Tölle, R., Lerchenberger, A., Wendl, M., Vogt, H., Calwer, H., Stetter, W., and Karg, F. New developments in Cu(In,Ga)(S,Se)$_2$ thin film modules formed by rapid thermal processing of stacked elemental layers. *Sol. Energy Mater. Sol. Cells* **90**, 3115–3123 (2006), doi: 10.1016/j.solmat.2006.06.031.

[16] Marudachalam, M., Hichri, H., Klenk, R., Birkmire, R. W., Shafarman, W. N., and Schultz, J. M. Preparation of homogeneous Cu(InGa)Se$_2$ films by selenization of metal precursors in H$_2$Se atmosphere. *Appl. Phys. Lett.* **67**(26), 3978–3980 (1995), doi: 10.1063/1.114424.

[17] Kim, K., Hanket, G. M., Huynh, T., and Shafarman, W. N. Three-step H$_2$Se/Ar/H$_2$S reaction of Cu-In-Ga precursors for controlled composition and adhesion of Cu(In,Ga)(Se,S)$_2$ thin films. *J. Appl. Phys.* **111**(8), 083710 (2012), doi: 10.1063/1.4704390.

[18] Hergert, F., Hock, R., Weber, A., Purwins, M., Palm, J., and Probst, V. In situ investigation of the formation of Cu(In,Ga)Se$_2$ from selenised metallic precursors by X-ray diffraction - the impact of gallium, sodium and selenium excess. *J. Phys. Chem. Solids* **66**(11), 1903–1907 (2005), doi: 10.1016/j.jpcs.2005.09.025.

[19] Kötschau, I. M., Kampmann, A., Hahn, T., Hinze, J., Pursche, O., Gorse, S., and Richter, E. Systematic design of an annealing process for Cu(In,Ga)Se$_2$ layer formation by in-situ XRD: A case study. In *25th European Photovoltaic Solar Energy Conference and Exhibition / 5th World Conference on Photovoltaic Energy Conversion, 6-10 September 2010, Valencia, Spain*, 3533–3537, (2010), doi: 10.4229/25thEUPVSEC2010-3BV.2.139.

[20] Kötschau, I., Gorse, S., Pursche, P., Hinze, J., Hahn, T., and Kampmann, A. Process and RTP equipment design for Cu(In,Ga)Se$_2$ layer formation using in-situ XRD techniques. In *Photovoltaic Specialists Conference (PVSC), 2011 37th IEEE*, 003321–003326, (2011), doi: 10.1109/PVSC.2011.6186650.

[21] Hanket, G., Shafarman, W., and Birkmire, R. Composition control in the growth of Cu(InGa)(SeS)$_2$ by the reaction of Cu-In-Ga precursors in H$_2$Se and H$_2$S. In *Photovoltaic Energy Conversion, Conference Record of the 2006 IEEE 4th World Conference on*, volume 1, 560–563, (2006), doi: 10.1109/WCPEC.2006.279517.

[22] Gremenok, V., Zaretskaya, E., Zalesski, V., Bente, K., Schmitz, W., Martin, R., and Moller, H. Preparation of Cu(In,Ga)Se$_2$ thin film solar cells by two-stage selenization

processes using N_2 gas. *Sol. Energy Mater. Sol. Cells* **89**(2-3), 129–137 (2005), doi: 10.1016/j.solmat.2004.11.014.

[23] Liao, K.-H., Su, C.-Y., and Ding, Y.-T. Effects of Ga accumulation on the microstructure of $Cu(In_{1-x},Ga_x)Se_2$ thin films during selenization. *J. Alloys Compd.* **581**(0), 250–256 (2013), doi: 10.1016/j.jallcom.2013.06.177.

[24] Purwins, M., Enderle, R., Schmid, M., Berwian, P., Müller, G., Hergert, F., Jost, S., and Hock, R. Phase relations in the ternary Cu-Ga-In system. *Thin Solid Films* **515**, 5895–5898 (2007), doi: 10.1016/j.tsf.2006.12.090.

[25] Hanket, G. M., Shafarman, W. N., McCandless, B. E., and Birkmire, R. W. Incongruent reaction of Cu-(InGa) intermetallic precursors in H_2Se and H_2S. *J. Appl. Phys.* **102**(7), 074922 (2007), doi: 10.1063/1.2787151.

[26] Walter, T. and Schock, H. Crystal growth and diffusion in $Cu(In,Ga)Se_2$ chalcopyrite thin films. *Thin Solid Films* **224**(1), 74–81 (1993), doi: 10.1016/0040-6090(93)90461-W.

[27] Kötschau, I. M. and Schock, H. W. Compositional depth profiling of polycrystalline thin films by grazing-incidence x-ray diffraction. *J. Appl. Crystallogr.* **39**, 683–696 (2006), doi: 10.1107/S002188980601987X.

[28] Rissom, T., Mainz, R., Kaufmann, C. A., Caballero, R., Efimova, V., Hoffmann, V., and Schock, H.-W. Examination of growth kinetics of copper rich $Cu(In,Ga)Se_2$-films using synchrotron energy dispersive X-ray diffractometry. *Sol. Energy Mater. Sol. Cells* **95**(1), 250–253 (2011), doi: 10.1016/j.solmat.2010.05.007.

[29] Boehnke, U.-C. and Kühn, G. Phase relations in the ternary system Cu-In-Se. *J. Mater. Sci.* **22**(5), 1635–1641 (1987), doi: 10.1007/BF01132385.

[30] Scragg, J. J. S., Choubrac, L., Lafond, A., Ericson, T., and Platzer-Björkman, C. A low-temperature order-disorder transition in Cu_2ZnSnS_4 thin films. *Appl. Phys. Lett.* **104**(4), 041911 (2014), doi: 10.1063/1.4863685.

[31] Müller, M., Dinnebier, R. E., and Schorr, S. A case study of parameterized rietveld refinement:the structural phase transition of $CuInSe_2$. *Z. Kristallogr.* **226**(12), 956–962 (2011), doi: 10.1524/zkri.2011.1407.

[32] Witte, W., Kniese, R., and Powalla, M. Raman investigations of $Cu(In,Ga)Se_2$ thin films with various copper contents. *Thin Solid Films* **517**(2), 867–869 (2008), doi: 10.1016/j.tsf.2008.07.011.

[33] Kambas, K., Julien, C., Jouanne, M., Likforman, A., and Guittard, M. Raman spectra of α- and γ-In_2Se_3. *phys. stat. sol. (b)* **124**(2), K105–K108 (1984), doi: 10.1002/pssb.2221240241.

[34] Emery, J., Julien, C., Jouanne, M., and Balkanski, M. Growth conditions and structure of polycrystalline InSe thin films. *Appl. Surf. Sci.* **33**, 619–624 (1988), doi: 10.1016/0169-4332(88)90360-1.

[35] Caballero, R., Izquierdo-Roca, V., Fontane, X., Kaufmann, C., Alvarez-Garcia, J., Eicke, A., Calvo-Barrio, L., Perez-Rodriguez, A., Schock, H., and Morante, J. Cu deficiency in multi-stage co-evaporated $Cu(In,Ga)Se_2$ for solar cells applications: Microstructure and Ga in-depth alloying. *Acta Mater.* **58**(9), 3468–3476 (2010), doi: 10.1016/j.actamat.2010.02.021.

[36] Xu, C.-M., Huang, W.-H., Xu, J., Yang, X.-J., Zuo, J., Xu, X.-L., and Liu, H.-T. Defect-induced structural disorder in tetragonal $Cu(In_{1-x}Ga_x)_5Se_8$ thin films investigated by raman spectroscopy: the effect of Ga addition. *J. Phys.: Condens. Matter* **16**(23), 4149–4155 (2004), doi: 10.1088/0953-8984/16/23/029.

[37] Delsol, T., Samantilleke, A. P., Chaure, N. B., Gardiner, P. H., Simmonds, M., and Dharmadasa, I. M. Experimental study of graded bandgap $Cu(InGa)(SeS)_2$ thin films grown on glass/molybdenum substrates by selenization and sulphidation. *Sol. Energy Mater. Sol. Cells* **82**(4), 587–599 (2004), doi: 10.1016/j.solmat.2004.02.018.

[38] Chichibu, S., Mizutani, T., Murakami, K., Shioda, T., Kurafuji, T., Nakanishi, H., Niki, S., Fons, P. J., and Yamada, A. Band gap energies of bulk, thin-film, and epitaxial layers of $CuInSe_2$ and $CuGaSe_2$. *J. Appl. Phys.* **83**(7), 3678–3689 (1998), doi: 10.1063/1.366588.

[39] Weber, A., Rodriguez, H., Mainz, R., Klaer, J., Pistor, P., Klenk, R., Klaus, M., Meeder, A., Neisser, A., and Schock, H. Fast $Cu(In,Ga)Se_2$ formation by processing Cu-In-Ga precursors in selenium atmosphere. In *37th IEEE Photovoltaic Specialist Conference (PVSC)*, 003315–003320, (2011), doi: 10.1109/PVSC.2011.6186649.

[40] Gödecke, T., Haalboom, T., and Ernst, F. Phase equilibria of Cu-In-Se I. Stable states and nonequilibrium states of the In_2Se_3-Cu_2Se subsystem. *Z. Metallkd.* **91**, 622–634 (2000).

[41] Predel, B. Cu-Ga (Copper-Gallium). In Cr-Cs - Cu-Zr, Madelung, O., editor, volume 5d of *Landolt-Börnstein - Group IV Physical Chemistry*, 1–8. Springer Berlin Heidelberg (1994), doi: 10.1007/10086090_1074.

[42] Witte, W., Abou-Ras, D., Albe, K., Bauer, G. H., Bertram, F., Boit, C., Brüggemann, R., Christen, J., Dietrich, J., Eicke, A., Hariskos, D., Maiberg, M., Mainz, R., Meessen, M., Müller, M., Neumann, O., Orgis, T., Paetel, S., Pohl, J., Rodriguez-Alvarez, H., Scheer, R., Schock, H.-W., Unold, T., Weber, A., and Powalla, M. Gallium gradients in $Cu(In,Ga)Se_2$ thin-film solar cells. *Prog. Photovolt: Res. Appl.* **in press** (2014).

[43] Pohl, J. and Albe, K. Thermodynamics and kinetics of the copper vacancy in CuInSe$_2$, CuGaSe$_2$, CuInS$_2$, and CuGaS$_2$ from screened-exchange hybrid density functional theory. *J. Appl. Phys.* **108**(2), 023509 (2010), doi: 10.1063/1.3456161.

[44] Pohl, J., Klein, A., and Albe, K. Role of copper interstitials in CuInSe$_2$: First-principles calculations. *Phys. Rev. B* **84**, 121201 (2011), doi: 10.1103/PhysRevB.84.121201.

[45] Wang, Y.-C. and Shieh, H.-P. D. Improvement of bandgap homogeneity in Cu(In,Ga)Se$_2$ thin films using a modified two-step selenization process. *Appl. Phys. Lett.* **103**(15), 153502 (2013), doi: 10.1063/1.4824762.

[46] Beck, M. E., Swartzlander-Guest, A., Matson, R., Keane, J., and Noufi, R. CuIn(Ga)Se$_2$-based devices via a novel absorber formation process. *Sol. Energy Mater. Sol. Cells* **64**, 135–165 (2000).

[47] Dejene, F. The structural and material properties of CuInSe2 and Cu(In,Ga)Se2 prepared by selenization of stacks of metal and compound precursors by Se vapor for solar cell applications. *Sol. Energy Mater. Sol. Cells* **93**(5), 577–582 (2009), doi: 10.1016/j.solmat.2008.12.002.

[48] Kamada, R., Shafarman, W. N., and Birkmire, R. W. Cu(In,Ga)Se$_2$ film formation from selenization of mixed metal/metal-selenide precursors. *Sol. Energy Mater. Sol. Cells* **94**(3), 451–456 (2010), doi: 10.1016/j.solmat.2009.11.004.

[49] Shi, J. H., Li, Z. Q., Zhang, D. W., Liu, Q. Q., Sun, Z., and Huang, S. M. Fabrication of Cu(In,Ga)Se$_2$ thin films by sputtering from a single quaternary chalcogenide target. *Prog. Photovolt: Res. Appl.* **19**(2), 160–164 (2011), doi: 10.1002/pip.1001.

[50] Liu, J., Zhuang, D., Luan, H., Cao, M., Xie, M., and Li, X. Preparation of Cu(In,Ga)Se$_2$ thin film by sputtering from Cu(In,Ga)Se$_2$ quaternary target. *Prog. Nat. Sci. Mat. Int.* **23**(2), 133–138 (2013), doi: 10.1016/j.pnsc.2013.02.006.

[51] Moon, D. G., Yun, J. H., Gwak, J., Ahn, S., Cho, A., Shin, K., Yoon, K., and Ahn, S. Cu(In,Ga)Se$_2$ thin films without Ga segregation prepared by the single-step selenization of sputter deposited Cu-In-Ga-Se precursor layers. *Energy Environ. Sci.* **5**(12), 9914–9921 (2012), doi: 10.1039/c2ee22804a.

[52] Dietrich, J., Abou-Ras, D., Rissom, T., Unold, T., Schock, H., and Boit, C. Compositional gradients in Cu(In,Ga)Se$_2$ thin films for solar cells and their effects on structural defects. *IEEE J. Photovolt.* **2**(3), 364–370 (2012), doi: 10.1109/JPHOTOV.2012.2190584.

[53] Wei, S.-H., Ferreira, L. G., and Zunger, A. First-principles calculation of the order-disorder transition in chalcopyrite semiconductors. *Phys. Rev. B* **45**, 2533–2536 (1992), doi: 10.1103/PhysRevB.45.2533.

[54] Genzel, C., Denks, I., Gibmeier, J., Klaus, M., and Wagener, G. The materials science synchrotron beamline EDDI for energy-dispersive diffraction analysis. *Nucl. Instr. Meth. Phys. Res. A* **578**(1), 23–33 (2007), doi: 10.1016/j.nima.2007.05.209.

[55] Rodriguez-Alvarez, H., Kötschau, I., and Schock, H. Pressure-dependent real-time investigations on the rapid thermal sulfurization of Cu-In thin films. *J. Cryst. Growth* **310**(15), 3638–3644 (2008), doi: 10.1016/j.jcrysgro.2008.05.005.